A CFD/CSD INTERACTION METHODOLOGY FOR AIRCRAFT WINGS

Manoj K. Bhardwaj* and Rakesh K. Kapania†
Virginia Polytechnic Institute and State University, Blackbsurg, VA 24061-0203
Eric Reichenbach‡
The Boeing Company, St. Louis, MO 63166
Guru P. Guruswamy§
NASA Ames Research Center, Moffett Field, CA 94035

Abstract

With advanced subsonic transports and military aircraft operating in the transonic regime, it is becoming important to determine the effects of the coupling between aerodynamic loads and elastic forces. Since aeroelastic effects can significantly impact the design of these aircraft, there is a strong need in the aerospace industry to predict these interactions computationally. Such an analysis in the transonic regime requires high fidelity computational fluid dynamics (CFD) analysis tools, due to the nonlinear behavior of the aerodynamics in the transonic regime and also high fidelity computational structural dynamics (CSD) analysis tools. Also, there is a need to be able to use a wide variety of CFD and CSD methods to predict aeroelastic effects. Since source codes are not always available, it is necessary to couple the CFD and CSD codes without alteration of the source codes. In this study, an aeroelastic coupling procedure is developed to determine the static aeroelastic response of aircraft wings using any CFD and CSD code with little code integration. The aeroelastic coupling procedure is demonstrated on an F/A-18 Stabilator using NASTD (an in-house McDonnell Douglas CFD code) and NASTRAN. In addition, the Aeroelastic Research Wing (ARW-2) is used for demonstration of the aeroelastic coupling procedure by using ENSAERO (NASA Ames Research Center

*Former Graduate Student, Member AIAA, Now Limited Term Staff, Sandia National Laboratories, P.O. Box 5800 MS-0439, Albuquerque, NM 87185-0439

†Professor, Associate Fellow AIAA, 215 Randolph Hall

‡Senior Project Engineer, Member AIAA

§Senior Research Scientist, Associate Fellow AIAA, Applied Computational Aerodynamics Branch, MS 258-1

CFD code) and a finite element wing-box code. The results obtained from the present study are compared with those available from an experimental study conducted at NASA Langley Research Center and a study conducted at NASA Ames Research Center using ENSAERO and modal superposition. The results compare well with experimental data.

Introduction

Traditionally, aircraft designers have viewed aeroelastic effects as undesirable. To avoid aeroelastic phenomena, the stiffness of the wing was increased by adding weight to the structure. Recently, there has been an increased interest in taking advantage of aeroelastic effects for roll control, load alleviation, and drag reduction while reducing the wing weight, as in the Active Flexible Wing[1,2] (AFW) and the Active Aeroelastic Wing[3] (AAW) programs. In addition, the accurate prediction of wind tunnel model static aeroelastic deformations is becoming increasingly important for transonic testing of transport aircraft.[4] Whether viewed as undesirable or desirable, it is becoming more important to predict static aeroelastic behavior of transport and fighter aircraft especially in the the transonic regime.

Advanced CFD tools are necessary to capture the nonlinear behavior of the aerodynamics in the transonic regime (shocks, vortices, separation). In this regime, the nonlinear nature of the aerodynamics makes load prediction difficult. The accuracy of the loads on a wing depends on the accuracy of the shock waves prediction.[5] Coupling of high fidelity CFD and CSD tools to solve aeroelastic problems has received interest only in the past few years. Huge computational power is required to make the use of such tools feasible. Continuous improvements in computer speed, memory, and architecture have, however, made solving these computationally intensive problems more cost effective.

Both uncoupled and coupled methods for solving these nonlinear systems of equations[6] exist. Aeroelastic problems of aerospace vehicles are often dominated by flow nonlinearities and at times by large structural deformations. Therefore, coupled approaches are necessary to solve such problems accurately.[7]

DISCLAIMER

Coupled approaches for solving aeroelastic problems are usually categorized in two ways: loosely or strongly coupled. The loosely coupled approaches can be integrated or modular. Integrated, loosely coupled methods alter the source code of either the CSD or CFD analysis tool by including the coupling schemes in either code. Though the codes are integrated, the CFD and CSD equations are not being altered and are solved independently. Modular, loosely coupled methods do not integrate the coupling schemes into either the CFD or CSD code. This allows the use of a variety of CFD/CSD codes.

Strongly or fully (single domain) coupled approaches require the solution of the CFD and CSD equations simultaneously which necessitates the reformulation of the equations of each discipline.[8] The numerical matrices associated with the structures are orders of magnitude stiffer than those associated with fluids. Thus, it is numerically inefficient or even impossible to solve both systems using a monolithic numerical scheme.[7] Recently, there have been renewed attempts to solve both fluids and structures in a single computational domain.[9,10] However, they have been limited to simple two-dimensional problems and have not proven to be better than the loosely coupled approach.

Guruswamy and Yang[6] demonstrated a loosely coupled approach to aeroelasticity. The fluids and structures were modeled independently and exchanged boundary information to obtain aeroelastic solutions. The fluids were modeled using finite-difference based transonic small disturbance (TSD) equations. The structures were modeled using finite element equations. The two disciplines were coupled to solve aeroelastic problems of two-dimensional airfoils. This loosely coupled or domain decomposition approach was shown to be efficient and accurate. This approach has been extended to three-dimensional problems and is incorporated into advanced aeroelastic codes as XTRAN3S,[11] ATRAN3S,[12] and CAP-TSD.[13] Guruswamy[14,15] also demonstrated the same technique by modeling fluids with Euler/Navier-Stokes equations on moving grids. Matching the CFD grid displacements with the CSD or finite element model response maintains the accuracy of this loosely coupled approach.

Several papers[4,16–25] have presented techniques for calculating aeroelastic solutions using loosely coupled high fidelity CFD and CSD methods. Often the coupling is integrated, allowing the two disciplines to exchange information at the boundaries in an efficient manner. However, this usually requires either the CFD or CSD code to be rewritten to add for the communication between the two separate disciplines.

The CSD analysis, in some of this work,[22,23] is performed using a modal analysis approach; this makes the exchange of boundary information easier. The loads need only to be calculated on the CFD grid points. As a direct result, not many algorithms have been presented for accurate transformation of pressures on the CFD grid to loads on the CSD nodes. Future work in analyzing complex wing-body structures will require the use of detailed finite element models and the use of direct finite element equations, not modal analyses. Therefore, an accurate load transformation scheme is needed.

Macmurdy *et al.*[26] obtained a static aeroelastic solution of an intermediate complexity wing (ICW) using Euler flow equations (ENSAERO) coupled with finite element equations. The finite element wing-box was modeled using a Wright Patterson Air Force Base structural analysis code, ANALYZE.[27] Static aeroelastic solutions were obtained by loosely coupling ENSAERO with ANALYZE in a modular manner. The twist and leading edge plunge are obtained from the structural response which are then applied to the CFD grid. The loads are calculated at the CFD grid points and are transferred to the CSD nodes using various schemes. The schemes do not transfer the loads accurately since some of the information is extrapolated.

Tzong *et al.*[28] presented a general method for calculating aero-structure interactions. An interface method based on finite element technology was used to exchange information between the CFD and CSD codes. The CFD analysis was performed using OVERFLOW[29] and a Douglas panel code.[30] The CSD response was calculated using a McDonnell Douglas Corporation finite element code. The interface method maps each CFD grid point to a host

finite element. The displacements and loads are transferred between the CFD grid point and the CSD nodes using the shape functions of the host finite element. A disadvantage of this approach is that the shape functions of the finite elements in the model might not be available to the user. In addition, the normal degrees of freedom might not be contained in the host finite element to transfer the boundary information accurately. This interface method has been integrated into the finite element code at Douglas. This again restricts a user's ability to use a CFD or a CSD code of her/his choice.

Two ways of transferring the pressures on the CFD grid to the CSD nodes are possible.[28] In the first method, pressures on the CFD grid are interpolated onto the CSD model and are integrated to obtain the forces on the CSD nodes. Tzong *et al.*[28] state that the inconsistency between the CFD and CSD models makes this conversion improper. The pressures can be converted to the CSD model, but the loads may not be integrated accurately since information about the true surface areas is often not available from the CSD model. In the second method, the forces at the CFD grid points are calculated by using the CFD grid information and then are transferred to the CSD nodes. This transfer calculates loads on the CSD nodes more accurately and is easier to implement. This is the method chosen in this study.

In the loosely coupled modular approach, boundary information between the CFD and CSD codes is exchanged through the codes' native files. Native files are the files required by the code as input and the files to which the output is written. The forces are obtained from the output of pressures from the CFD code. A pressure mapping algorithm transfers the pressures from the CFD grid to the CSD nodes. The CSD code calculates the response of the structure. The resulting output, the displacements, are interpolated to the CFD grid using a displacement mapping algorithm. The CFD code calculates the flow field about this new CFD grid. The procedure is repeated in an iterative manner until a specified convergence criterion is met. Therefore, two mappings are necessary to obtain static aeroelastic solutions in a loosely coupled and modular manner. The mappings used are described later.

The mapping of the displacements from the CSD nodes to the CFD grid requires an interpolation scheme. Smith *et al.*[31] presented a review of the methodologies used to do this mapping in interfacing CFD/CSD codes. A significant literature review and an industry/government survey narrowed the search to six schemes: (i) the Infinite-plate spline; (ii) Finite-plate spline; (iii) Multiquadric-Biharmonic; (iv) Thin-Plate Spline; (v) Inverse Isoparametric Mapping; and (vi) Non-Uniform B-Splines. These methods were analyzed by a series of mathematical test cases and selected applications. The infinite-plate spline (IPS) method, commonly referred to as the Harder and Desmarais surface spline,[32] was chosen to interpolate displacements from the CSD nodes to the CFD grid. The IPS method provides reasonable results without having the requirement that the input grid be a rectangular array. In addition, its ease of use and implementation make it one of the better methods as can be seen by its use in several codes. More details of the other methods can be found in an excellent review given in Ref. [31].

Several researchers have investigated either artificial structural damping[33] or underrelaxation techniques[21,28] to converge the solution faster and/or to keep it stable. In this paper, an initial rigid steady state solution of the lifting surface is used to decrease the time to calculate a static aeroelastic solution as opposed to starting impulsively from free stream boundary conditions. In addition, the CFD solution need not be fully converged after each grid deformation before exchanging information with the structural analysis code. This has a similar effect as an underrelaxation scheme and has been used effectively as seen in Ref. [34].

Static aeroelastic solutions are obtained in this paper assuming a linear structural model. The loads obtained from the pressures are applied to the original finite element model to obtain the displacements. The finite element model is not regenerated using the displacements in the previous iteration although this capability is not difficult to include in the aeroelastic coupling procedure.

In this work, an aeroelastic coupling procedure is presented by which static aeroelastic solutions of aircraft wings are obtained. The aeroelastic coupling procedure requires only the grid point coordinates of the CFD and CSD grids to create the interface mappings. To demonstrate this procedure, a static aeroelastic solution of the F/A-18 Stabilator is calculated by using Euler flow equations as available in NASTD (an in-house McDonnell Douglas Aerospace - East code) and finite element equations as available in the structural analysis tool NASTRAN.[35] The solution is obtained in the highly nonlinear transonic range at Mach 0.95, and at one degree angle of attack. Next, two different CFD and CSD codes are used to obtain a static aeroelastic solution for the Aeroelastic Research Wing (ARW-2). Navier-Stokes equations, as available in ENSAERO,[36] are coupled with a finite element wing-box code to obtain a static aeroelastic solution in the transonic regime at Mach 0.85, at one and two degrees angle of attack. The flexible solutions are also compared with experimental results, and good agreement is obtained. The examples use direct finite element equations, not modal analysis equations, to obtain the structural response. The advantage of the proposed aeroelastic coupling procedure is thus shown by using two different sets of CFD/CSD codes to perform static aeroelastic analyses.

Due to space restrictions, all of the details and figures are not shown as these can be found in Ref. [37].

Aeroelastic Coupling Procedure

A static aeroelastic solution of a wing is obtained using the following aeroelastic coupling procedure:

1 Obtain an intermediate or rigid steady state CFD solution for the wing

2 Calculate the pressures at the CFD grid points on the aerodynamic surface

3 Map pressures at the CFD grid points to forces on the CSD nodes

4 Obtain the structural response of the wing

5 Map displacements at the CSD nodes to the displacements on the CFD grid points of the aerodynamic surface

6 Deform the entire CFD grid

7 Repeat steps 1-6 until preselected convergence criteria is met

The above steps, also shown in Fig. 1, are repeated in an iterative manner until a converged solution is obtained. This fixed-point iteration scheme is used for its simplicity and for its application to obtaining loosely coupled CFD/CSD solutions. To use a method which converges faster, like Newton's method,[38] large amounts of computational time would have to be spent in calculating sensitivities of pressure with respect to deformations. Direct finite element analysis, not modal analysis, determines the structural response; thus the number of unknowns makes this process inefficient. Therefore Newton's method is computationally too expensive to make this approach feasible.

In obtaining the static aeroelastic solution of a wing, either a fully converged rigid steady state solution is obtained or an intermediate solution is obtained before initiating the aeroelastic coupling procedure. In this paper, both methods were used. However, the aeroelastic solution converges faster if the aeroelastic coupling is started with the CFD rigid steady state solution as opposed to starting impulsively from free stream boundary conditions. Alternatively, introducing the structural coupling into the CFD solution process from the start, before obtaining even an intermediately converged CFD solution on the rigid wing, can cause serious problems leading to the possibility of a divergent solution.

The aerodynamic pressures are calculated using any CFD code. The forces are calculated at each CFD grid point using the pressures and calculated areas. The forces at the CFD grid points of the wing are then mapped onto the CSD nodes. To do this, each CFD grid point is mapped to a structural triangle. Using Fig. 2, step 1 shows the area used to obtain the force at CFD grid point i, j as indicated by the dotted box. Here it is assumed that the CFD grid is denser than the CSD grid. The four closest structural nodes are obtained using the upper or lower surface structural grid depending on which surface the CFD grid point is located. All possible triangles are formed using the four CSD nodes. Triangles that

do not contain the CFD point as an interior point are eliminated. The area coordinates of the CFD point i, j with respect to the structural triangle determine whether the point is an interior point. If the area coordinates sum to 1.0 ± 0.01, the CFD grid point is interior to the structural triangle. From Fig. 2, there are four triangles and triangles 1 and 2 do not contain the CFD grid point and therefore are eliminated. Of the remaining triangles, the distance, v_i, between the CFD grid point i, j and each CSD node of triangle m is calculated as,

$$v_i^m = \sqrt{(x_p^m - x_a)^2 + (y_p^m - y_a)^2 + (z_p^m - z_a)^2} \quad \text{For } i = 1, 3 \tag{1}$$

where (x_a, y_a, z_a) are the coordinates of the CFD grid point i, j and (x_p^m, y_p^m, z_p^m) are the coordinates of CSD node p of triangle m. The largest vertex distance for each triangle m is obtained as

$$w_{max}^m = max(v_1^m, v_2^m, v_3^m) \tag{2}$$

where max is the maximum of the values v_1^m, v_2^m, v_3^m. The triangle with the smallest value of w_{max} is the "smallest" structural triangle for CFD point i, j; thus the forces at CFD grid point i, j are mapped to this triangle.

Four CSD nodes were used to show this mapping algorithm, but this number, n_{clo}, can be increased to any number depending on the density of the finite element grid. It is possible not to find a structural triangle for a CFD grid point if this number is too low. For example, if all four nodes in the previous example are to the same side of the CFD grid point, then none of the formed triangles would contain the CFD grid point. In this paper, $n_{clo} = 20$ is used. This number was validated by graphically viewing the mapping of the CFD grid points to the structural triangles for various choices of n_{clo}.

The structural response of the system is calculated using the forces obtained above on the CSD nodes. The following system of equations are solved,

$$[K]\{u_s\} = \{f_s\} \tag{3}$$

where $\{u_s\}$ are the displacements at the CSD nodes, and $\{K\}$ is the stiffness matrix of the CSD or finite element model. This can be solved by any structural analysis tool to obtain the displacements, $\{u_s\}$, on the CSD nodes.

The displacements, $\{u_a\}$, on the aerodynamic portion of the CFD grid are calculated using the structural response, $\{u_s\}$. A surface spline[32] is used to interpolate the displacements from the CSD nodes to the CFD grid points. Reasonable accuracy[39] is obtained as long as extrapolation is avoided. The surface spline equation is derived from the governing equations of a plate of infinite extent that deforms in bending only. The surface spline system of equations becomes

$$[A^s]\{c\} = \{u_{spl}\} \tag{4}$$

where $[A^s]$ is dependent on the coordinates of the spline points, $\{c\}$ is the vector of unknown coefficients of the surface spline equation, and $\{u_{spl}\}$ are the displacements at the spline points. In the preprocessing stage, some of the structural nodes and CFD farfield grid points are chosen as the spline points. Matrix $[A^s]$ is formed using the coordinates of the chosen spline points. The displacements for the CFD farfield spline points are fixed at zero while the remainder of the spline point displacements, $\{u_{spl}\}^s$, are extracted from the structural response, $\{u_s\}$, as

$$\{u_{spl}\}^s = [E]\{u_s\} \tag{5}$$

Here $[E]$, composed of zeroes and ones, is a $n_{spl} \times n_{max}$ matrix where n_{spl} is the number of structural spline points and n_{max} is the number of CSD nodes. Matrix $[A^s]$ is decomposed using an LU factorization. The coefficients of the surface spline, $\{c\}$, are solved by forward and backward substitutions.

The displacements at the CFD surface grid points, $\{u_a\}$, are calculated by using the coordinates of the CFD grid points within the surface spline equation. The exterior CFD grid is deformed using the CFD surface grid displacements, $\{u_a\}$, but the deformation of the exterior CFD grid depends on the aerodynamic analysis code being used. Two separate

codes for fluid analysis are used in this paper. One of the codes, ENSAERO,[36] has a built in scheme to move the grid once the CFD surface grid is deformed. The other, NASTD,[40] does not have such a scheme. So a simple grid moving scheme was applied when NASTD was used.

The aeroelastic coupling procedure is demonstrated by calculating a flexible solution of an F/A-18 Stabilator and the Aeroelastic Research Wing (ARW-2).

Examples

Next, the details of the static aeroelastic analyses of the F/A-18 Stabilator and the Aeroelastic Research Wing (ARW-2) are presented and compared with experimental and other available computational data.

F/A-18 Stabilator: CFD and CSD Modeling

For the F/A-18 Stabilator, Euler flow equations, as available in NASTD, are used to demonstrate the aeroelastic coupling procedure. The analysis is performed at sea-level, one degree angle of attack, and at Mach 0.95. The CFD grid of the F/A-18 Stabilator is approximately 800,000 grid points. The CFD surface grid of the F/A-18 Stabilator only is shown in Fig. 3.

A general purpose finite element program, NASTRAN, is used in analyzing the structure. The stiffness matrix produced by NASTRAN is used to obtain the displacements for given aerodynamic loads. During the linear aeroelastic analysis procedure, NASTRAN is not directly involved, since the stiffness matrix does not change during the procedure. The finite element model of the F/A-18 Stabilator consists of 2000 nodes and 12000 d.o.f.

F/A-18 Stabilator: Aeroelastic Coupling Procedure

The first step in the aeroelastic coupling procedure is obtaining the CFD solution for the lifting surface. For this case, the rigid steady state solution is obtained before the aeroelastic analysis cycle begins. Once the CFD solution is obtained, the forces on the CSD grid are calculated using the preprocessed mapping. The mapping of the CFD points to the structural

triangles as previously discussed is shown in Fig. 4. Here the mapped structural triangle for each CFD point is presented. The structural triangle does not refer to an actual structural element. So shape functions are not necessary, and if linear displacements are assumed over each element, then energy is conserved during the mapping. The actual structure of the wing does not extend to the wing root, but this was done to avoid computational problems with the CFD code NASTD.

Since NASTD does not have a built-in grid generator the exterior CFD grid has to be deformed using the deflections on the wing surface. There are two ways of doing this: (i) regenerate a completely new CFD exterior grid or (ii) deform the existing CFD grid. Often, the existing CFD grid is deformed. These methods redistribute points along grid lines that are in the radial direction normal to the surface by displacing them a value equal to the surface value times a some spacing parameter. Guruswamy[7] used a normalized arc length as the spacing parameter. Batina[23] represented the exterior grid using a spring network, where the stiffness of the spring is inversely proportional to the length of the side of the CFD cell. This prevents the CFD grid from losing its quality. In this paper, only vertical displacements are taken into account. Therefore, a simple cosine spacing function is used to deform the exterior grid normal to the wing surface.

Assuming the CFD grid for this case has the i index varying circumferentially around the wing section, the j index varying in the normal direction, and the k index varying along the span. Once the surface deflections are known at j =1, a cosine spacing function is used to deform the exterior grid at each spanwise (k = constant face) location. The spacing function, dependent on the location along the normal direction , i.e. the j index, is defined as

$$\alpha_s^j = \cos\frac{\pi(j-1)}{2(j_{max}-1)} \quad \text{For} \quad j = 1, j_{max} \tag{6}$$

where j_{max} is the maximum number of points extending in the radial direction normal to the surface. Using the displacements at the CFD surface grid, i.e. $j = 1$, the exterior grid is deformed at each k = constant surface by multiplying the surface displacement by the

spacing parameter, α_s. The new vertical coordinate at some j section is,

$$z_{i,k}^{new} = z_{i,k}^{rigid} + \alpha_s^j u_{i,k}^{j=1} \tag{7}$$

Only the vertical displacements are taken into account. Note that the $z_{i,k}^{rigid}$ coordinates are used and not the z coordinates from the previous iteration. To avoid overlapping of the CFD grid, a minimum spacing criteria, α_{min} is chosen as,

$$\alpha_{min} = fs * (\alpha_s^1 - \alpha_s^2) \tag{8}$$

where $\alpha_s^1 = 1$ and fs is subjectively chosen to prevent loss of grid quality. For this analysis, fs is chosen in the range of 1-2. Parameter α_s^2 depends on j_{max}. This assumes the grid is stretching smoothly away from the surface. If the spacing between two consecutive points is smaller than α_{min}, $z_{i,k}^{j+1} - z_{i,k}^{j} < \alpha_{min}$, then α_s is set to one for that entire j section. In this example, all the points within the $j = 26$ boundary are moved the same amount as the aerodynamic surface at $j = 1$. All the points exterior to $j = 26$, i.e. $26 < j < j_{max}$, are moved using Eqn. 6. This enforces that the outer boundaries of the CFD grid do not move. This is done to take advantage of distributed computing capabilities in the future where the grid can be broken into many zones. A Hewlett-Packard workstation was used to perform the calculations.

Aeroelastic Research Wing (ARW-2): CFD and CSD Modeling

The Aeroelastic Research Wing (ARW-2), a supercritical airfoil with aspect ratio of 10.3 and a leading edge sweep of 28.8°, is used to validate the force and displacement mappings. The strong conservation law form of the thin-layer Reynolds-averaged Navier-Stokes equations are used to calculate the fluid flow about the ARW-2 wing as available in ENSAERO. The structural response is calculated by the finite element wing-box code. The aeroelastic solution is obtained at Mach 0.85, $\alpha = 1$ and 2 degrees, $q = 200$ psf, and is compared with experimental results. In addition, the results are also compared with another similar work, which uses modal analysis as opposed to the direct finite element analysis used in this study.

The CFD code uses a C-H type grid with a grid size of 171 (circumferentially) x 51 (spanwise) x 45 (normal) points. The wing CFD grid is shown in Fig. 5. The wing has a grid size of 139 (circumferentially) x 39 (spanwise) points. The fluid flow equations are solved for Mach 0.85, an angle of attack, α, of 1 and 2 degrees, and a free stream dynamic pressure, q, of 200 psf.

The finite element wing-box model of the ARW-2 wing uses Allman's triangular elements in conjunction with axial bars to represent the wing's spars, ribs, and skins. Figure 6 shows the spars and ribs of the ARW-2 wing. The wing is discretized into a 11 x 13 mesh, 312 nodes, 1872 d.o.f. The ARW-2 wing consists of composite fiberglass skins, but the finite element wing-box code does not yet have composite capability. An equivalent isotropic wing is created by matching bending and twisting properties with the ARW-2 wing made of composite fiberglass skins. Details of the composite skin ARW-2 wing finite element model can be obtained in Ref. [41]. Details of the isotropic equivalent of the composite skin ARW-2 are available in Ref. [37].

Aeroelastic Research Wing (ARW-2): Aeroelastic Coupling Procedure

The aeroelastic coupling procedure is more integrated using ENSAERO and the finite element wing-box code since the source codes were available. If only the vertical displacements are taken into account for the F/A-18 Stabilator and ARW-2 wing, the CFD grid can become distorted. Therefore, ENSAERO uses the vertical deflections to calculate a rigid body rotation and a deflection so as to avoid this problem when dealing with the ARW-2 wing. This was also done for the F/A-18 Stabiltor using NASTD. This means that chordwise rigidity is assumed for the wing. This is a good approximation for the ARW-2 wing. Byrdsong *et al.* measured experimental data for the flexible ARW-2, and state that the ARW-2 has sufficient chordwise rigidity. A Cray-90 was used to obtain the solution for this case.

Results

F/A-18 Stabilator

The convergence of the aeroelastic solution for the F/A-18 Stabilator is monitored in several ways. The L_2 norm of the residuals of the continuity, momentum, and energy equations are examined. The loads on the wing surface are also examined. Satisfying these two criteria helps assure that the CFD solution is converged. In the CSD solution, the displacements at various locations are examined to assure convergence. One of the convergence checks for the structural analysis is shown in Fig. 7, where the deflection of the wing tip of the F/A-18 Stabilator is plotted after each cycle of the aeroelastic coupling procedure. The structural solution converges very quickly. This is because the rigid steady state solution was obtained prior to initiating the aeroelastic coupling procedure. In addition, the aeroelastic effect is not significant; the largest displacement on the F/A-18 Stabilator is 1.55 inches.

The final converged flexible F/A-18 Stabilator is shown in Fig. 8 with the initial undeformed rigid F/A-18 Stabilator. The largest deflection occurs at the trailing edge tip of the F/A-18 Stabilator, approximately 1.5 inches. From a previous analytical study (performed at McDonnell Douglas) using CAP-TSD, a transonic small disturbance CFD code, coupled with modal analysis structures, the largest deflection of the F/A-18 Stabilator was calculated to be 1.56 inches. The deflection using NASTD coupled with NASTRAN is also about 1.55 inches. The present results do compare well with existing data. Unfortunately, more details of the comparisons are not available.

Next, the Aeroelastic Research Wing (ARW-2), is used to determine the accuracy of the entire aeroelastic coupling procedure, since experimental static aeroelastic data exist for it.

Rigid Steady State Solution

The first step is to obtain the rigid steady state solution for the two cases. i.e. the one and two degree angle of attack cases. Intermediate rigid steady state solutions were obtained by using Navier-Stokes flow equations as available in ENSAERO. Convergence of the rigid steady state solutions is checked by examining the L_2 norm of the residuals of the fluids equations. The L_2 norm is not sufficiently reduced, but this is done since a completely

converged solution is not necessary to start the aeroelastic coupling. This study and the Farhangnia *et al.*[42] study start with the same rigid steady state solution of the ARW-2 using ENSAERO. Farhangnia *et al.* use the first five mode shapes as opposed to the direct finite element equations used in the work. Since final results are compared later, the starting rigid steady state solutions are also compared by examining Fig. 9. The figure shows the C_p variation at the 70.7% semi-span location. Because both studies used ENSAERO to obtain the rigid steady state solution, the results match as expected.

After initiating the aeroelastic coupling procedure, the CFD solution convergence is checked by examining the L_2 norm of the residual of the fluids equations, while the CSD solution is checked by examing displacements at various locations on the wing structure. Flexible steady state solutions are obtained at $\alpha = 1$ and 2 deg. C_p variation at the 70.7% semi-span location, for the flexible ARW-2 wing, is shown in Fig. 10 and plotted with experimental data from Ref. [42]. The C_p variation compares well with the experimental data. The shock location for the experimental data is 5% of chord aft of the computational data.

Due to the flexibility, the shock location has moved aft in both the one and two degree angle of attack cases. The C_p plot at the 70.7% semi-span location is shown in Fig. 11 verifies this for $\alpha = 2$ deg case. For $\alpha = 1$ deg case, the shock movement is less.

Figures 12 and 13 show the deflections of the front spar for one degree and two degree angle of attack cases, respectively. Experimental data from Byrdsong *et al.*[43] is also shown. The wing tip for the one degree case deflects approximate six inches, while the wing tip for the two degree case deflects approximately eight inches. Good agreement is obtained using direct finite element data coupled with Navier-Stokes flow equations.

In addition, Fig. 14 also shows aeroelastic data from Farhangnia *et al.*[42] where modal analysis was used for structural analysis for the one degree case. Modal analysis results are about 25% in error at the wing tip, where the first five mode shapes were used. Finite element equations results are 3% in error compared to experimental data. Here it is shown

the increased accuracy of using direct finite element displacement data as opposed to modal analysis data. Again, the accuracy of the aeroelastic coupling procedure and the finite element wing-box code are demonstrated successfully.

Conclusions

An aeroelastic coupling procedure was presented whereby static aeroelastic analysis can be performed by allowing the coupling of a wide variety of computational fluid dynamics (CFD) codes and computational structural dynamics (CSD) codes. The procedure was demonstrated by performing static aeroelastic analysis on an F/A-18 Stabilator by using finite element capability in NASTRAN coupled with Euler flow equations as available in NASTD (an in-house McDonnell Douglas CFD code). In addition, the Aeroelastic Research Wing (ARW-2) was used to validate the aeroelastic coupling procedure by using a finite element wing-box code coupled with Navier-Stokes equations as available in ENSAERO (NASA Ames Research Center CFD code). Experimental data were used to compare the computational aeroelastic solution of the ARW-2 and good agreement was obtained. The increased accuracy of the use of direct finite element displacement data as opposed to modal analysis was also shown. The advantage of this aeroelastic coupling procedure is that it only requires the grid points of the CSD and CFD grids. Using only the grid point locations, necessary mappings are created to be able to obtain static aeroelastic solutions. This procedure is modular. Currently, only the vertical displacements are considered. Therefore, the interpolation scheme can be changed to account for the in-plane displacements. The aeroelastic coupling procedure is not as efficient as a completely integrated scheme. This procedure is also limited in that large amounts of deformation will cause the problems with CFD grid deformation. This will occur at points near divergence speeds. However, for swept back wings, divergence is not a problem.

Acknowledgements

Portions of this work were performed under a NASA Ames-Virginia Tech Consortium

#NCC2-5097 and a McDonnell Douglas Contract #PO Z60807. The authors would like to thank Vic Spain, Chansup Byun, Rudy Yurkovich, and Mehrdad Farhangnia for their help and guidance.

References

[1] Yurkovich, R., "Optimum Wing Shape for an Active Flexible Wing," *AIAA Paper 95-1220*, April 1995.

[2] Perry III, B., Cole, S. R., and Miller, G. D., "A Summary of the Active Flexible Wing Program," *AIAA Paper 92-2080*, 1992.

[3] Andersen, G., Forster, E., Kolonay, R., and Eastep, F., "Multiple Control Surface Utilization in Active Aeroelastic Wing Technology," *Journal of Aircraft*, **Vol. 34**, No. 4, July-August 1997, pp. 552–557.

[4] Hooker, J. R., Burner, A. W., and Valla, R., "Static Aeroelastic Analysis of Transonic Wind Tunnel Models Using Finite Element Methods," *AIAA Paper 97-2243*, June 1997, Presented at the 15th Applied Aerodynamics Conference.

[5] Murty, H. S. and Johnson, G. W., "Nonlinear Aspects of Transonic Aeroelasticity," *Canadian Aeronautics and Space Journal*, **Vol. 39**, No. 2, June 1993, pp. 78–84.

[6] Guruswamy, G. P. and Yang, T. Y., "Aeroelastic Time-Response Analysis of Thin Airfoils by Transonic Code LTRAN2," *Computers and Fluids*, **Vol. 9**, No. 4, December 1980, pp. 409–425.

[7] Guruswamy, G. P., "Coupled Finite-Difference/Finite-Element Approach for Wing-Body Aeroelasticity," *AIAA Paper 92-4680*, September 1992.

[8] Bauchau, O. A. and Ahmad, J. U., "Advanced CFD and CSD Methods for Multidisciplinary Applications in Rotorcraft Problems," *AIAA Paper 96-4151*, July 1996.

[9] Bendiksen, O. O., "A New Approach to Computational Aeroelasticity," *AIAA Paper 91-0939*, April 1991.

[10] Felker, F. F., "A New Method for Transonic Static Aeroelastic Problems," *AIAA Paper 92-2123*, April 1992.

[11] Borland, C. J. and Rizzetta, D., "XTRAN3S - Transonic Steady and Unsteady Aerodynamics for Aeroelastic Applications, Volume 1-Theoretical Manual," *AFWAL-TR-80-3017*, December 1985.

[12] Guruswamy, G. P., Goorjian, P. M., and Merritt, F. J., "ATRAN3S - An Unsteady Transonic Code for Clean Wings," *NASA TM 86783*, December 1985.

[13] Batina, J. T., Bennett, R. M., Seidal, D. A., Cunningham, S. R., and Bland, S. R., "Recent Advances in Transonic Computational Aeroelasticity," *NASA TM 100663*, September 1988.

[14] Guruswamy, G. P., "Unsteady Aerodynamic and Aeroelastic Calculations of Wings Using Euler Equations," *AIAA Journal*, **Vol. 28**, No. 3, March 1990, pp. 461–469.

[15] Guruswamy, G. P., "Vortical Flow Computations on Swept Flexible Wings Using Navier-Stokes Equations," *AIAA Journal*, **Vol. 28**, No. 12, December 1990, pp. 2077–2084.

[16] Guruswamy, G. P. and Byun, C., "Fluid-Structural Interactions Using Navier-Stokes Flow Equations Coupled with Shell Finite Element Structures," *AIAA Paper 93-3087*, July 1993.

[17] Guruswamy, G. P. and Byun, C., "Direct Coupling of Euler Flow Equations with Plate Finite Element Structures," *AIAA Journal*, **Vol. 33**, No. 2, February 1995, pp. 375–377.

[18] Yeh, D. T., "Aeroelastic Analysis of a Hinged-Flap and Control Surface Effectiveness Using the Navier-Stokes Equations," *AIAA Paper 95-2263*, June 1995.

[19] Nathman, J. K. and Barton, J. M., "Aeroelastic Calculations with an Euler Code," *AIAA Paper 97-2271*, June 1997, Presented at the 15th Applied Aerodynamics Conference.

[20] Robinson, B. A., Batina, J. T., and Yang, H. T. Y., "Aeroelastic Analysis of Wings Using the Euler Equations with a Deforming Mesh," *AIAA Paper 90-1032*, April 1990.

[21] Chipman, R., Walters, C., and MacKenzie, D., "Numerical Computation of Aeroelastically Corrected Transonic Loads," *AIAA Paper 79-0766*, 1979.

[22] Rausch, R. D., Batina, J. T., and Yang, H. T. Y., "Three-Dimensional Time-Marching Aeroelastic Analyses Using an Unstructured Euler Method," *NASA TM 107567*, March 1992.

[23] Batina, J. T., "Unsteady Euler Algorithm with Unstructured Dynamic Mesh for Complex-Aircraft Aeroelastic Analysis," *AIAA Paper 89-1189*, April 1989.

[24] Purcell, T. W., Borland, C. J., and Tinoco, E. N., "Non-Linear Aeroelastic Predictions of Transport Aircraft," *AIAA Paper 90-1852*, 1990.

[25] Schuster, D., Vadyak, J., and Atta, E., "Static Aeroelastic Analysis of Fighter Aircraft Using a Three-Dimensional Navier-Stokes Algorithm," *AIAA Paper 90-0435*, January 1990.

[26] Macumurdy, D., Kapania, R., and Guruswamy, G. P., "Static Aeroelastic Analysis of Wings Using Euler/Navier-Stokes Equations Coupled with Wing-Box Finite Element Structures," *AIAA Paper 94-1587*, April 1994.

[27] Venkayya, V. B. and Tischler, V. A., "ANALYZE - Analysis of Aerospace Structures with Membrane Elements," *AFFDL-TR-78-170*, December 1978.

[28] Tzong, G., Chen, H. H., Chang, K. C., Wu, T., and Cebeci, T., "A General Method for Calculating Aero-Structure Interaction on Aircraft Configurations," *AIAA Paper 96-3982*, September 1996.

[29] Buning, P. G., Chan, W. M., Renze, K. J., Sondak, D., Chiu, I. T., and Slotnick, J. P., "OVERFLOW User's Manual, Version 1.6," NASA Ames Research Center, 1991.

[30] Hess, J. L., Friedman, D. M., and Clark, R. W., "Calculation of Compressible Flow About Three-Dimensional Inlets with Auxiliary Inlets, Slats, and Vanes by Means of a Panel Method," *NASA CR 174975*, 1985.

[31] Smith, M. J., Hodges, D. H., and Cesnik, C. E. S., "An Evaluation of Computational Algorithms to Interface between CFD and CSD Methodologies," *Report WL-TR-96-3055*, November 1995.

[32] Harder, R. L. and Desmarais, R. N., "Interpolation Using Surface Splines," *Journal of aircraft*, **Vol. 9**, No. 2, October 1971, pp. 189–191.

[33] Obyashi, S. and Guruswamy, G. P., "Convergence Acceleration of a Navier-Stokes Solver for Efficient Static Aeroelastic Computations," *AIAA Journal*, **Vol. 33**, No. 6, June 1995, pp. 1134–1141.

[34] Neuman III, J. C., "Efficient Nonlinear Static Aeroelastic Wing Analysis," *Submitted to Computers and Fluids*, December 1996.

[35] MacNeal, R. H., "The NASTRAN Theoretical Manual," *NASA SP-221(01)*, April 1971.

[36] Guruswamy, G. P., "ENSAERO - A Multidisciplinary Program for Fluid/Structural Interaction Studies of Aerospace Vehicles," *Computing Systems in Engineering*, **Vol. 1**, No. 2-4, 1990, pp. 237–257.

[37] Bhardwaj, M. K., *A CFD/CSD Interaction Methodology for Aircraft Wings*, Ph.D. thesis, Virginia Polytechnic Institute and State University, Blacksburg, VA, October 1997.

[38] Burden, R. L. and Faires, J. D., *Numerical Analysis*, chap. 2, PWS-KENT Publishing Company.

[39] Rodden, W. P., McGrew, J. A., and Kalman, T. P., "Comment on 'Interpolation Using Surface Splines'," *Journal of aircraft*, **Vol. 9**, No. 12, December 1972, pp. 869–871.

[40] Bush, R. H., "A Three Dimensional Zonal Navier-Stokes Code for Subsonic Through Hypersonic Propulsion Fields," *AIAA Paper 88-2830*, 1988.

[41] Sanford, M. C., Seidel, D. A., Eckstrom, C. V., and Spain, C. V., "Geometrical and Structural Properties of an Aeroelastic Research Wing (ARW-2)," *NASA TM 4110*, April 1989.

[42] Farhangnia, M., Guruswamy, G. P., and Biringen, S., "Transonic-Buffet Associated Aeroelasticity of a Supercritical Wing," *AIAA Paper 96-0286*, January 1996.

[43] Byrdsong, T. A., Adams, R. R., and Sanford, M. C., "Close-range Photogrammetric Measurement of Static Deflections of an Aeroelastic Supercritical Wing," *NASA TM 4194*, 1990.

[44] Bisplinghoff, R. L., *Principles of Aeroelasticity*, Dover Publications, Inc.

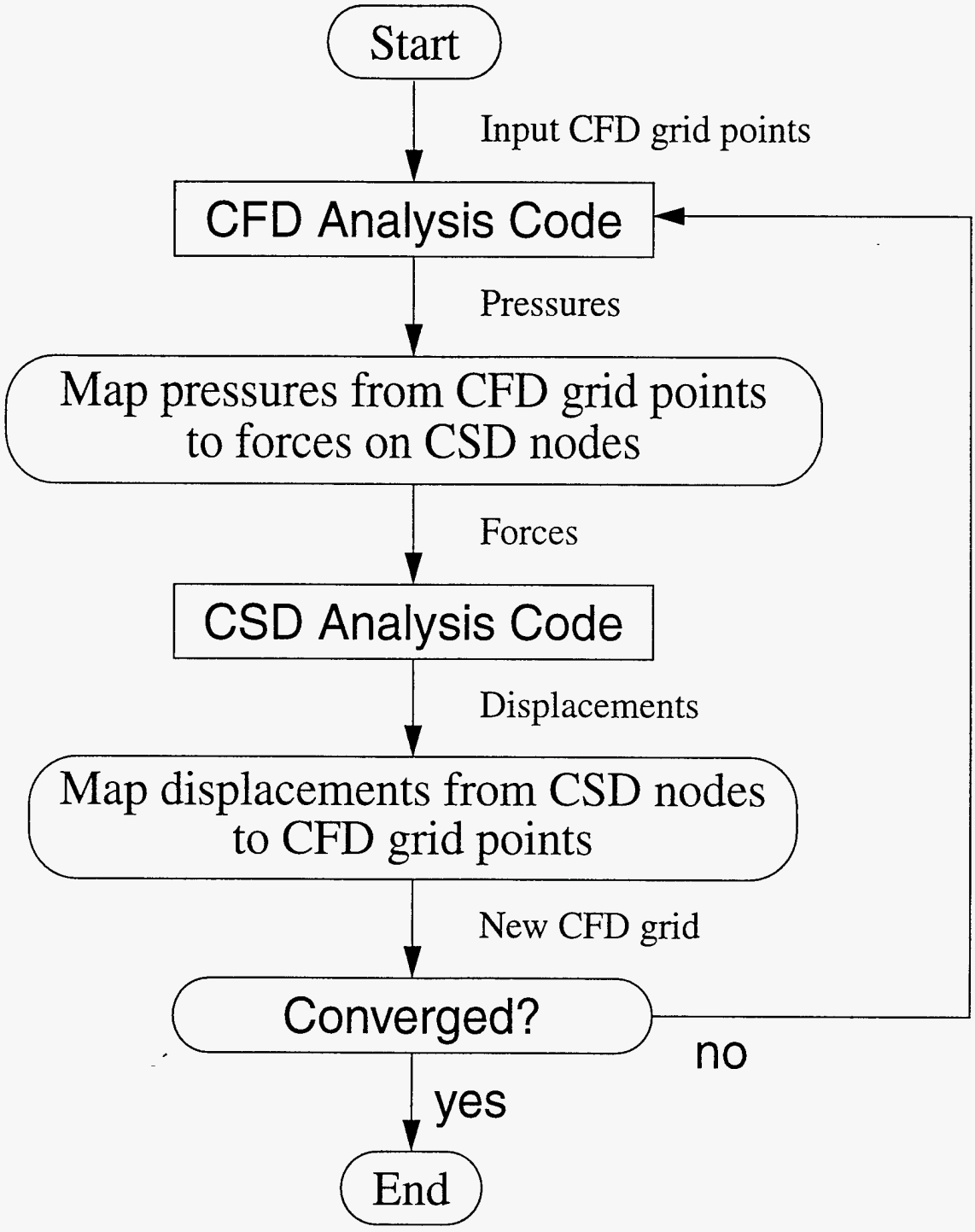

Figure 1: Flow Chart of Aeroelastic Coupling Procedure

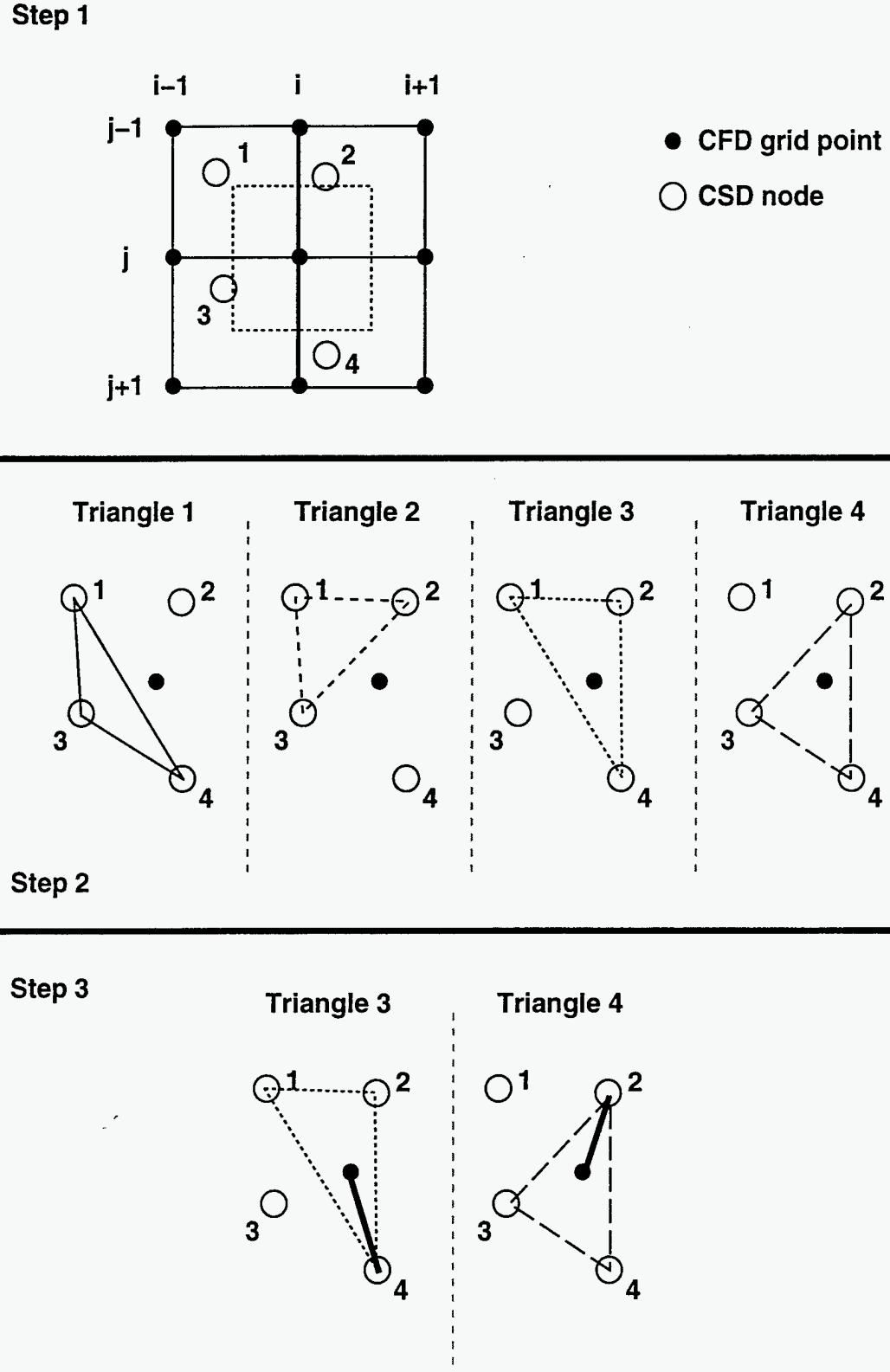

Figure 2: Mapping of a CFD Grid Point to a CSD Triangle

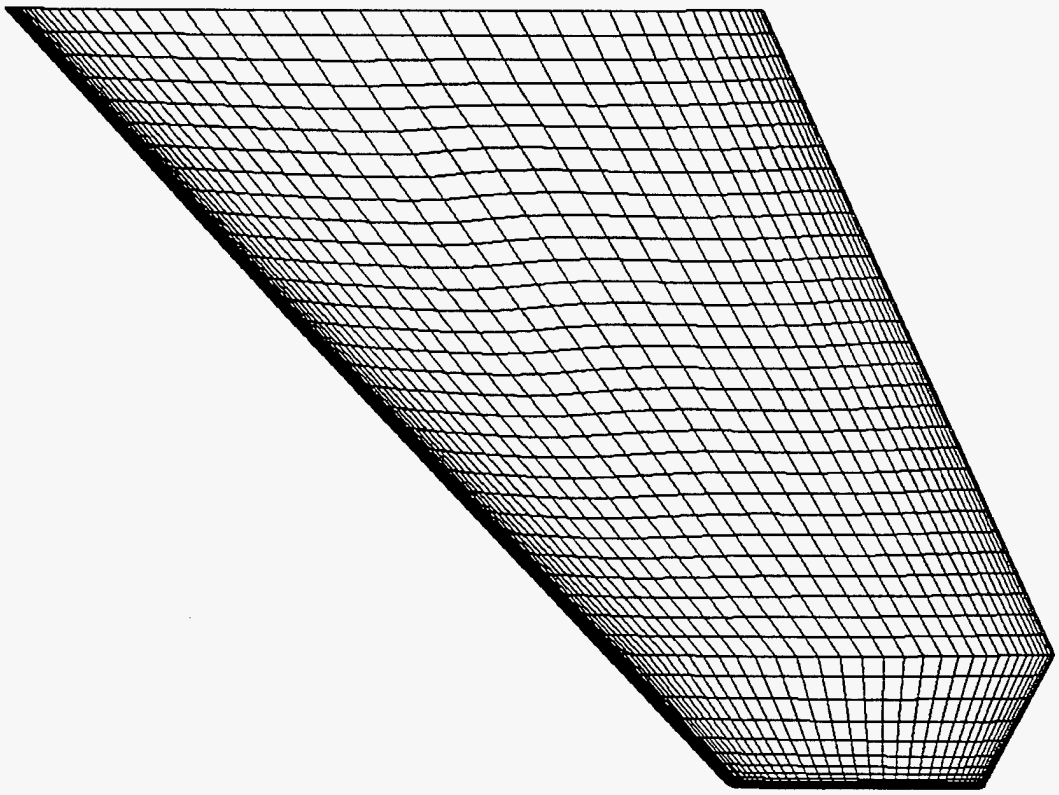

Figure 3: CFD Grid for the F/A-18 Stabilator

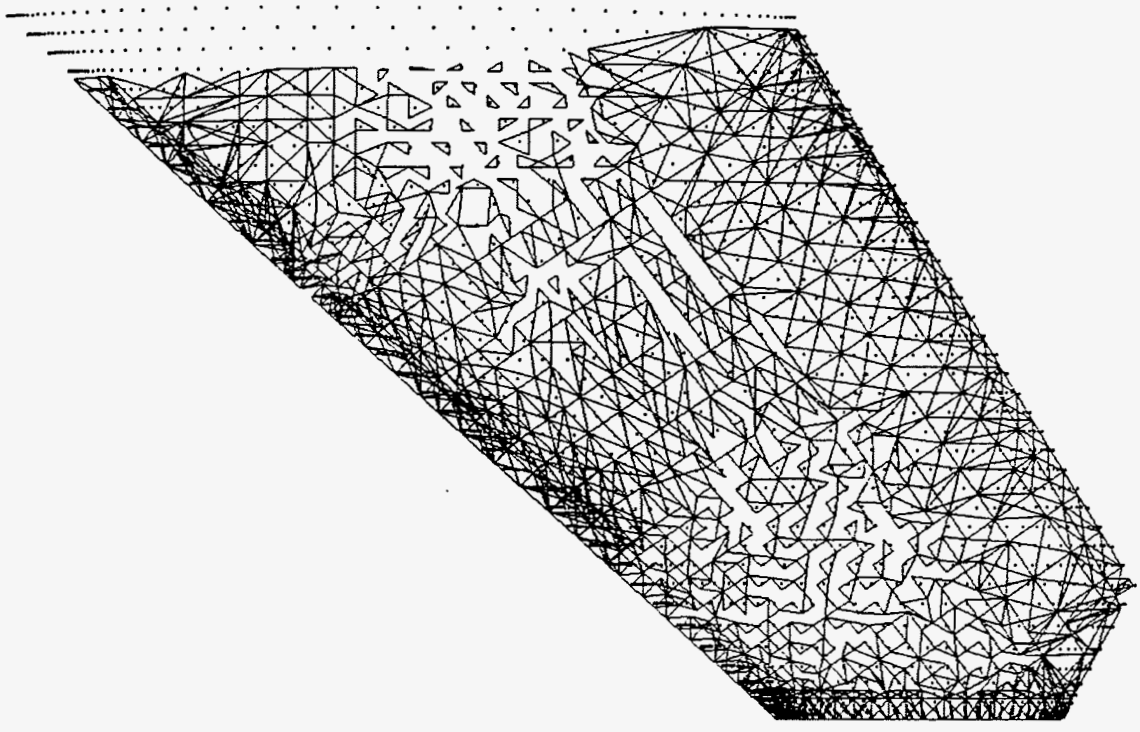

Figure 4: Mapping of CFD Points to Structural Triangles for the F/A-18 Stabilator

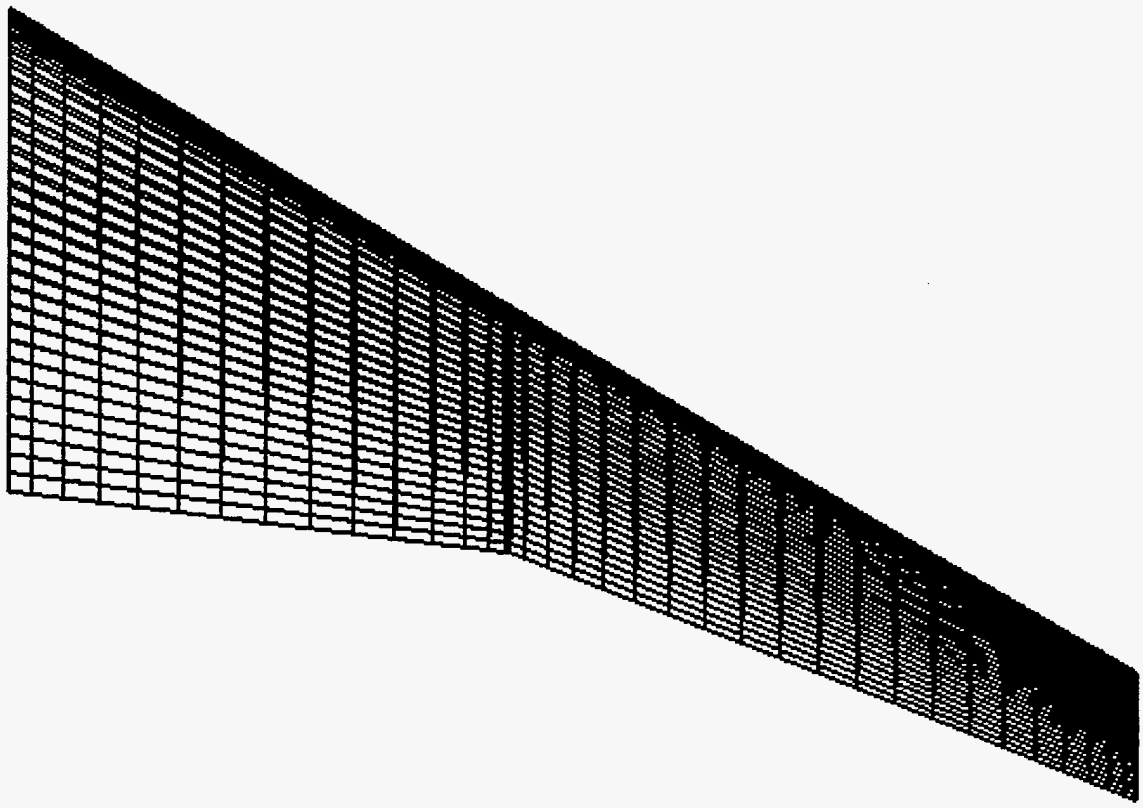

Figure 5: CFD Grid of the ARW-2 Wing

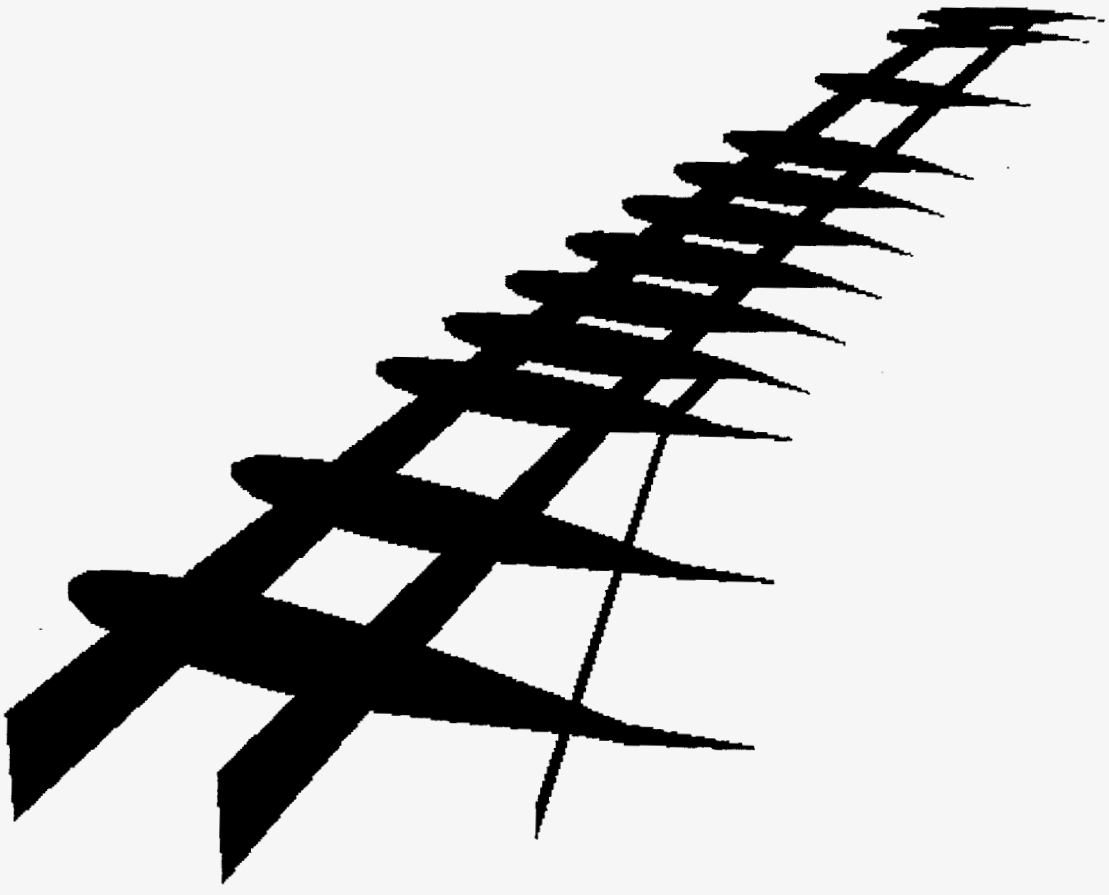

Figure 6: Finite Element Model of the Spars and Ribs of the ARW-2 Wing

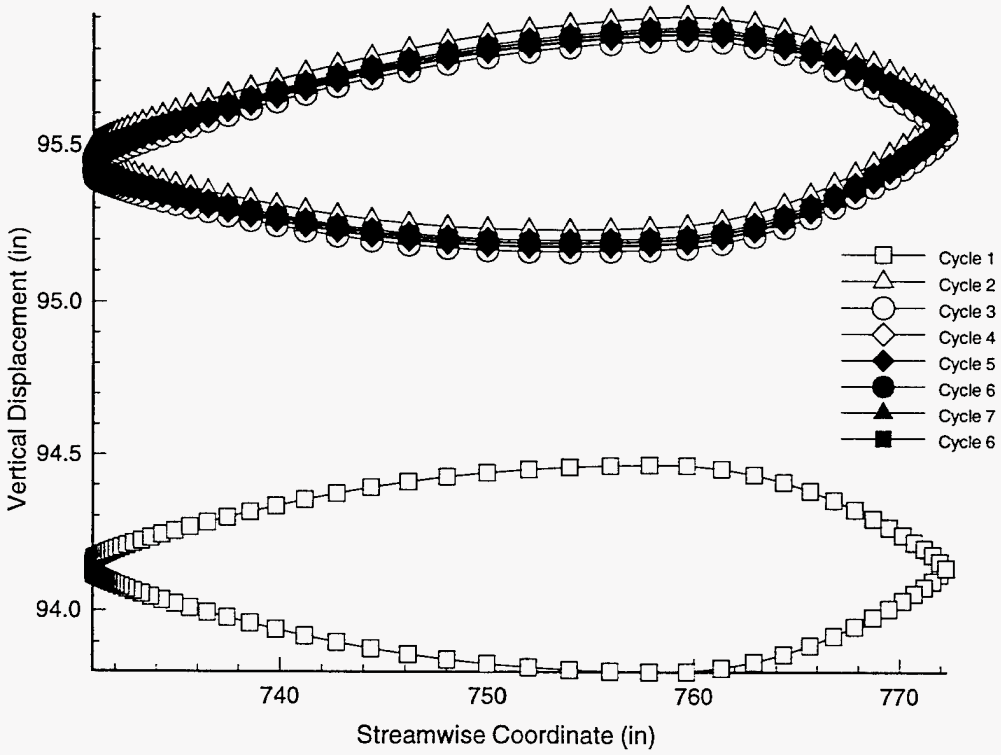

Figúre 7: Convergence of the Wing Tip of the F/A-18 Stabilator

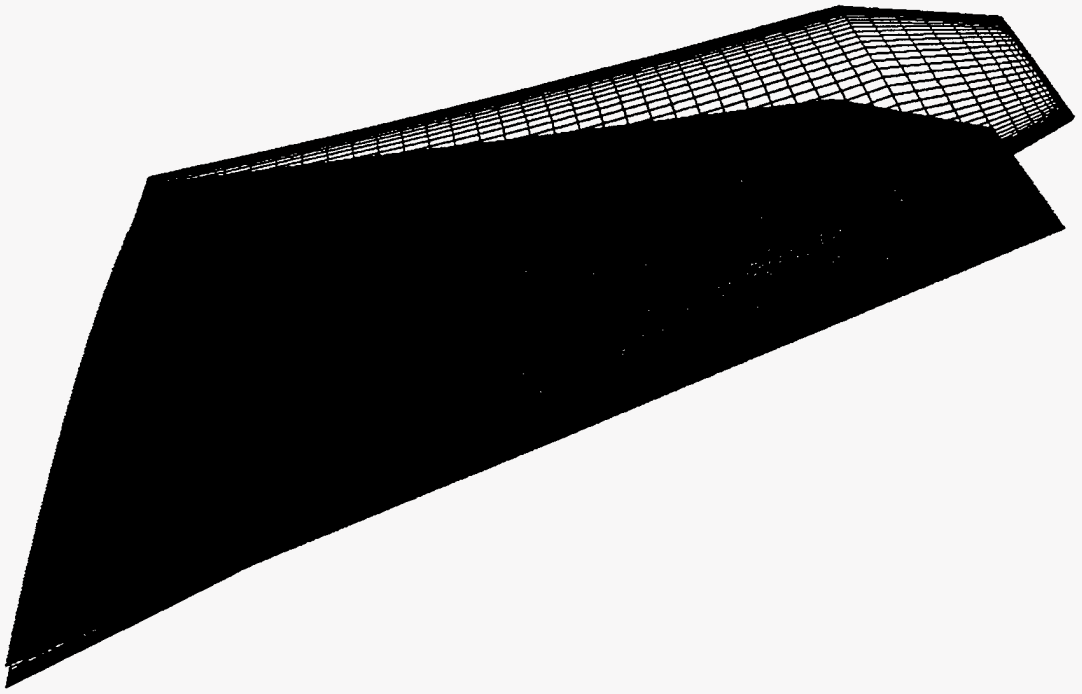

Deflections scaled by a factor of 10

Figure 8: Final Converged and Initial Undeflected F/A-18 Stabilator

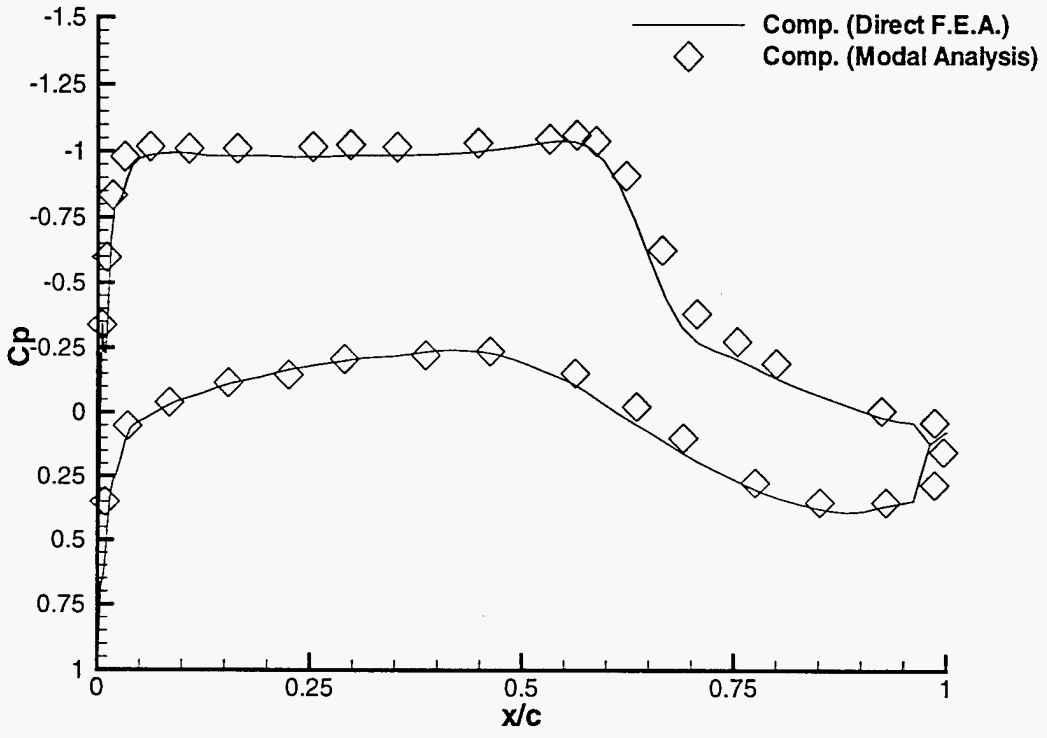

Figure 9: Comparison of C_p Variation for Rigid Steady State Solution at the 70.7% Semi-span Location for $\alpha = 1$ deg

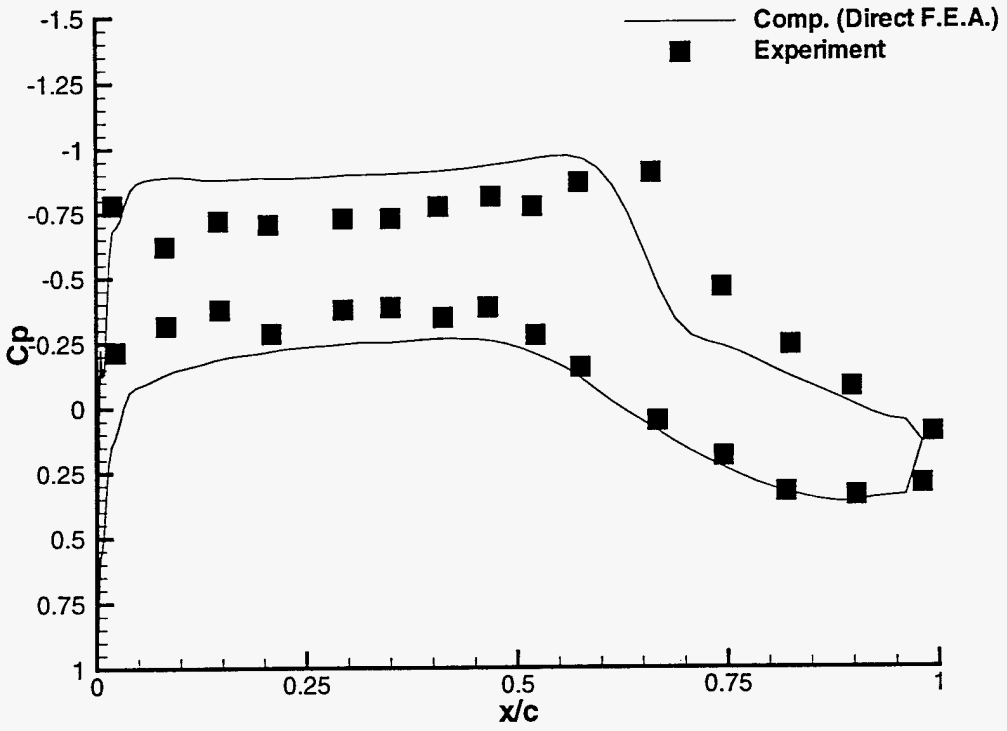

Figure 10: Comparison of C_p Variation of Experimental Data Versus Computational Results at the 70.7% Semi-span Location for $\alpha = 1$ deg

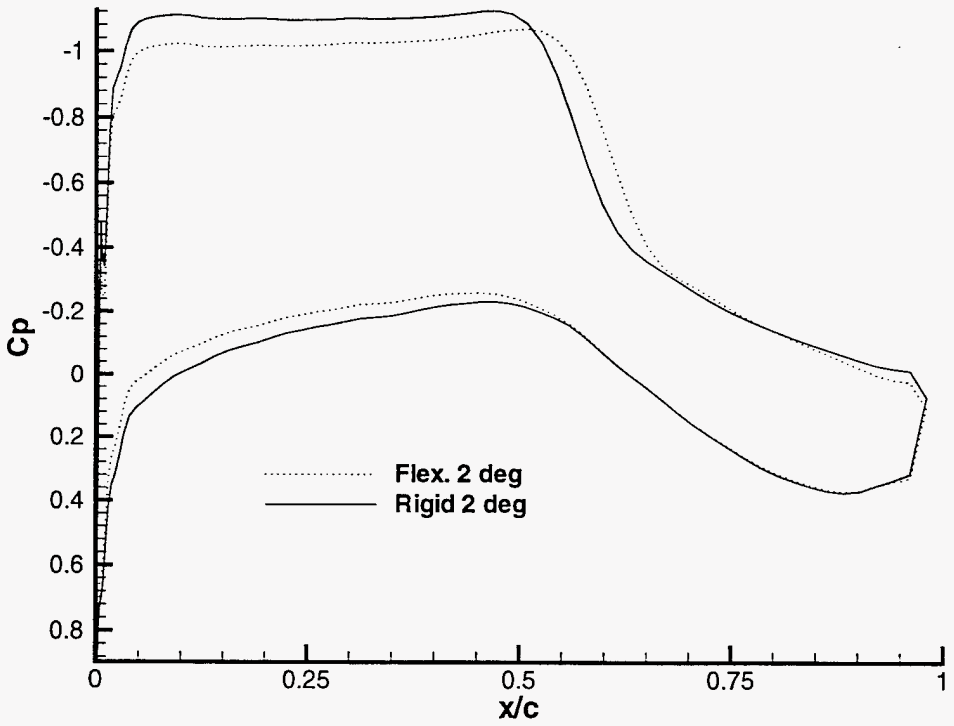

Figure 11: C_p Variation for $\alpha = 2$ deg at the 70.7% Semi-span Location

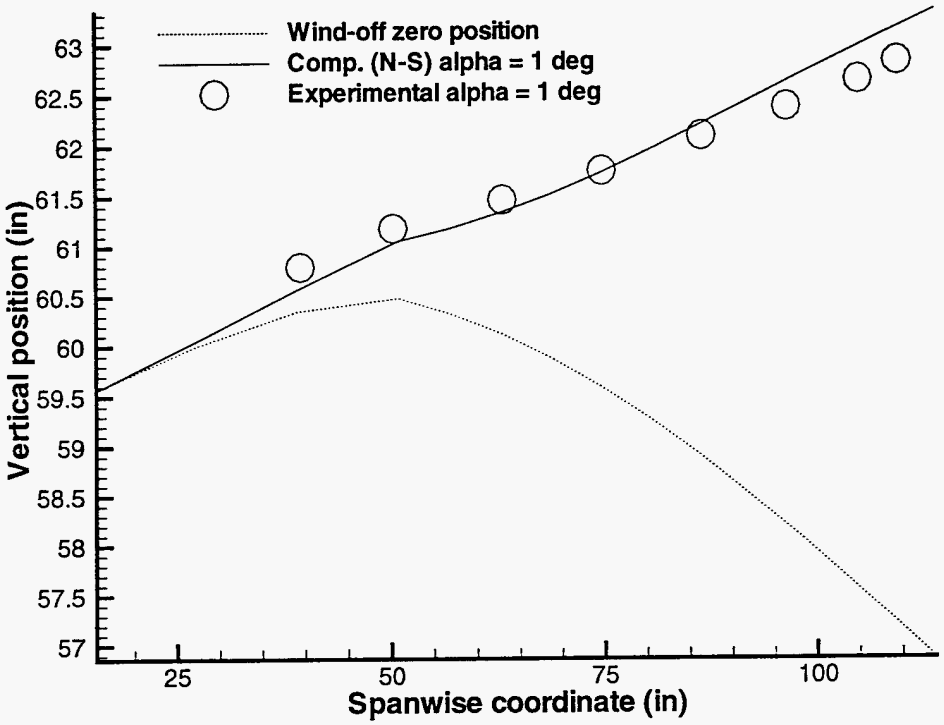

Figure 12: Comparison of the Experimental and Computational Front Spar Deflections of the ARW-2 Wing at $\alpha = 1$ deg

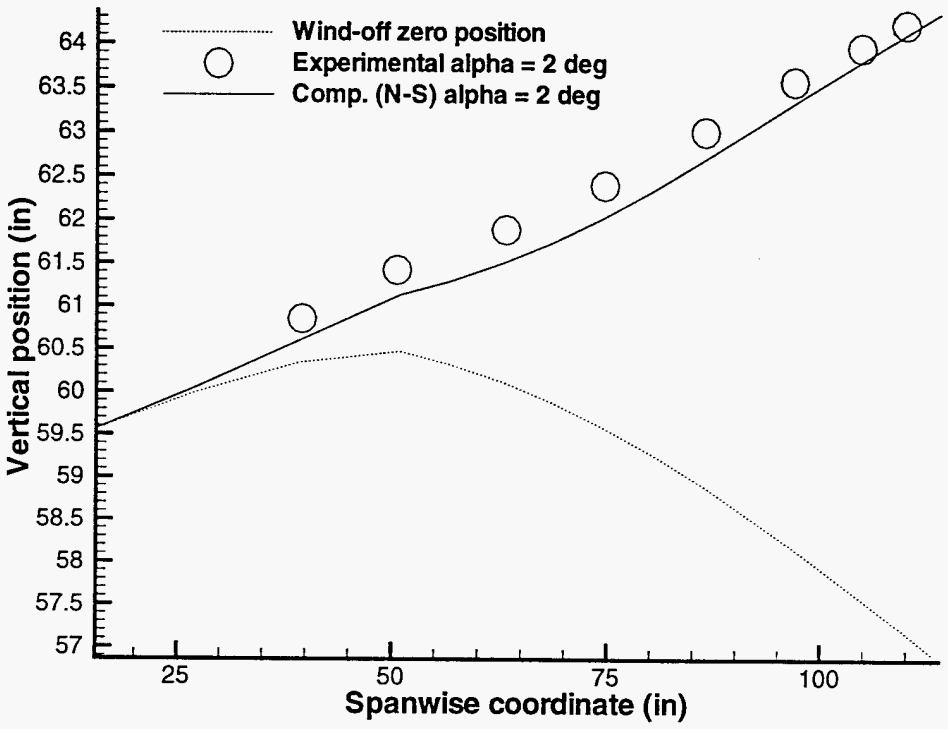

Figure 13: Comparison of the Experimental and Computational Front Spar Deflections of the ARW-2 Wing at $\alpha = 2$ deg

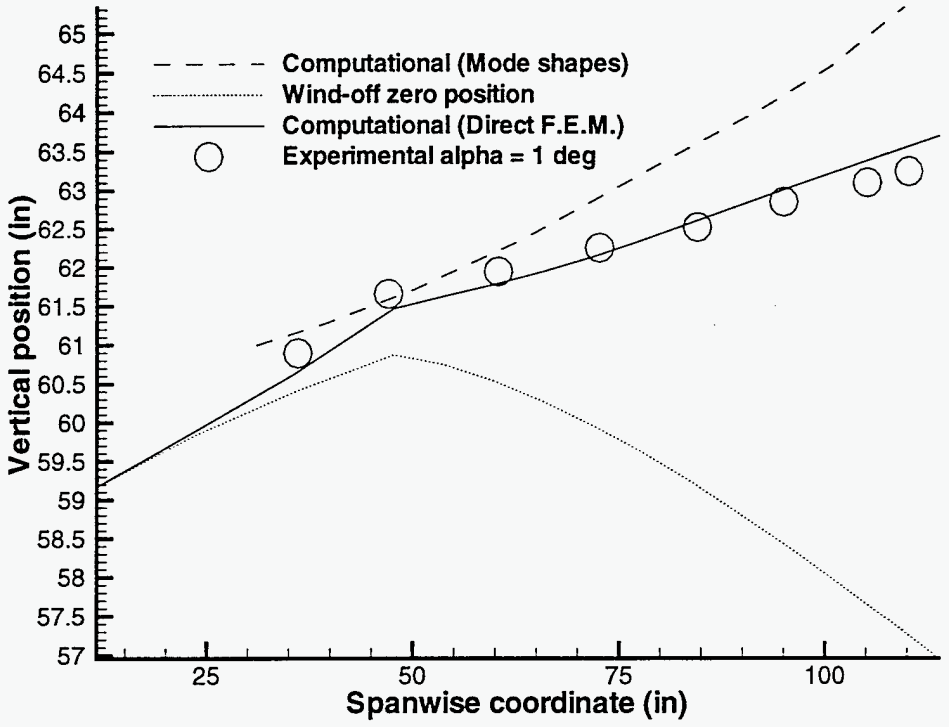

Figure 14: Comparison of the Rear Spar Deflections Using Modal Analysis Versus Finite Element Analysis of the ARW-2 Wing at $\alpha = 1$ deg

Report Number (14) SAND--98-0136C
CONF-980909--

Publ. Date (11) 199801
Sponsor Code (18) DOE/DP, XF
UC Category (19) UC-700, DOE/ER

DOE